SPACE OPERATION AND PERFORMANCE OF DOPED GERMANIUM PHOTO-CONDUCTING DETECTORS IN THE FAR INFRARED: EXPERIENCE FROM THE ISO LWS

BRUCE SWINYARD
Space Science Department, Rutherford Appleton Laboratory,
Chilton, Didcot, Oxon,
U.K. OX11 OQX

PETER CLEGG, SARAH LEEKS, MATT GRIFFIN
Queen Mary and Westfield College, University of London,
Mile End Road, London,
U.K. E1 4NS

TANYA LIM[1], MARTIN BURGDORF
ISO Science Operations Centre, Space Science Department of ESA,
Villafranca, P.O. Box 50727,
28080, Madrid,
Spain

ABSTRACT. The performance of the ten doped germanium photoconducting detectors on the Infrared Space Observatory Long Wavelength Spectrometer is discussed. This instrument was designed to make spectroscopic measurements of astronomical sources in the wavelength range from 43 to 198 μm. It employed[2] a combination of stressed and unstressed Ge:Ga detectors and one Ge:Be detector coupled to Infrared Labs JF-4 integrating amplifiers. The performance of the detectors was affected by the ionising radiation in the space environment. The Noise Equivalent Power of the detectors increased by a factor of ~4 compared to that measured during ground testing. We show that this was the result of reducing the operating bias, and therefore the responsivity, of the detectors and using shorter integration ramps to alleviate the effects of the ionising radiation impacts.

1 Introduction

The cold focal plane unit of the LWS consisted of a grating spectrometer working in first order to cover the range from 84 to 196.9 μm and second order from 43 to 93 μm; two Fabry-Perot interferometers, mounted on an interchange wheel, covering respectively 47 - 70 μm and 70 - 196.9 μm; and collimating and re-imaging optics to focus the beam on to a detector sub-system that consisted of ten doped germanium photo-conductors. The grating performed order sorting for the Fabry-Perots and the grating itself was order sorted using broad band filters mounted in front of the detectors. There were five detectors covering the grating first order, each with a pass band of approximately 20 μm, and five covering the second order, each with a pass band of approximately 10 μm. Three types of detector were used: Ge:Be for the shortest wavelength channel (43 to 50 μm), denoted SW1; unstressed Ge:Ga for the five channels covering 50 to 110 μm, denoted SW2, SW3, SW4, SW5 and LW1 respectively; and stressed Ge:Ga for the four

[1] Now at Rutherford Appleton Laboratory.
[2] ISO exhausted its helium supply on 8 April 1998

channels covering 110 to 196.9 μm, denoted LW2, LW3, LW4 and LW5. All the detectors were 1x1x1 mm. The Ge:Be and unstressed Ge:Ga detectors were operated at 3.0 K and the stressed Ge:Ga at 1.8 K. All ten detectors were read out using JF-4 integrating amplifiers supplied by Infrared Laboratories, Inc. The outputs of the integrating amplifiers were sampled at 88 Hz and the amplifiers reset at 0.25, 0.5 or 1 second intervals. The relative response of each detector was monitored using infrared illuminators also supplied by Infrared Laboratories, Inc. A full description of the instrument and its operation is given in Clegg *et al.*(1996) and a complete description of the detector subsystem and its ground testing in Church *et al.*(1993).

The instrument had two basic modes of operation: the grating mode and the Fabry-Perot mode. In the grating mode the interchange wheel was set to provide a clear aperture and the grating was rotated about its central axis by means of a servo controlled drive mechanism. The scan range was determined by the wavelength range required for the particular observation; to scan the entire wavelength range of the LWS a rotation of $\pm 7^{o}$ was required. In the Fabry-Perot mode the interchange wheel was used to place one or other of the Fabry-Perots in the collimated part of the beam through the instrument. One of the Fabry-Perots could also be placed in the beam and deliberately misaligned to make measurements under the darkest conditions possible; this was referred to as the opaque mode.

The overall performance of the LWS has been described by Swinyard *et al.* (1996 and 1998), and the long term performance of the detectors in the space environment by Lim *et al.* (1998). In the latter paper it is shown that, whilst the responsivity of the detectors changed linearly with time around the orbit as a result of the dose of ionising radiation received by the detectors, this was curable by breaking down the detectors using a high bias voltage (see also Price *et al.* 1992). Further it is shown that the responsivity of the detectors did not significantly change over the two and a half years of the mission and that the measured dark current was not affected by the increasing dose of ionising radiation. The latter result was contrary to those of Price *et al.* (1992) whose ground tests showed that the dark current behaved in the same manner as the responsivity when the detectors were irradiated.

In the current paper we concentrate on the performance of the detectors in terms of Noise Equivalent Power (NEP), responsivity and the effects of the space environment on the choice of the operating parameters for the detectors and instrument operations. We also describe the method used to extract the photocurrent from the raw amplifier output and describe briefly the method used to correct for the non-linear response of the detectors in the presence of high input fluxes.

2 Performance and operation

2.1 Extraction of Photocurrent

Figure 1 shows the equivalent circuit for the detectors and the associated read out electronics. In this system, the photocurrent from a detector causes a build up of charge on the integrating node of its amplifier, producing an increasing output voltage which represents the input flux. The voltage across the input capacitance of the FET leads to a drop in the net bias voltage across the

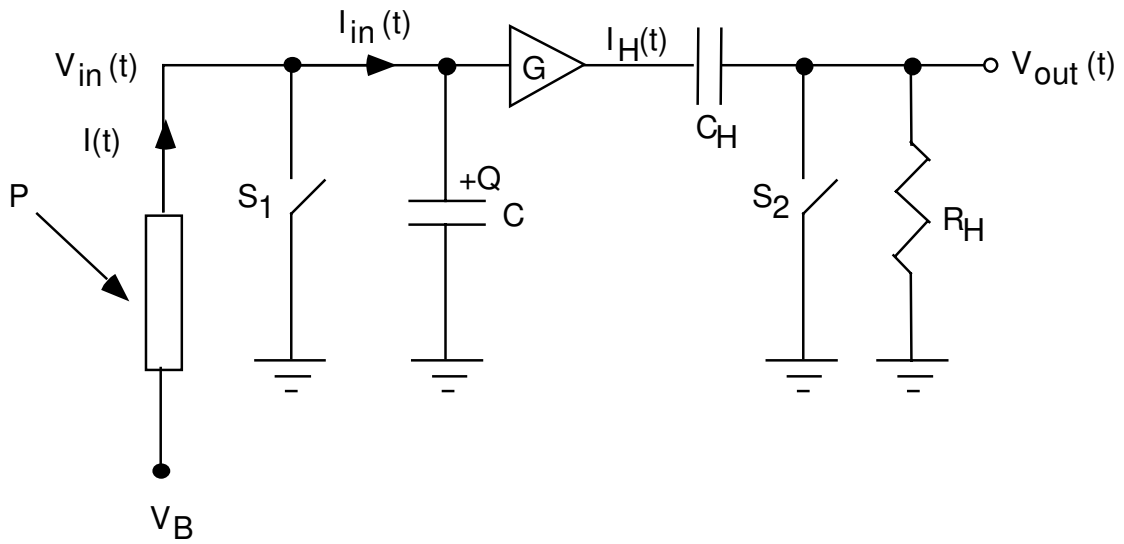

Figure 1: The equivalent circuit of the detector and read out electronics. C is the input capacitance of the integrating JF4 amplifier, S_1 represents the reset/compensation circuit, G represents the gain of all elements of the circuit up to the high-pass filter formed by C_H and R_H, P is the power falling on the detector and I(t) is the total current flowing through the detector.

detector, changing its resistance and responsivity. The change in responsivity under these circumstances can be characterised by a de-biasing parameter defined as

$$a = \frac{1}{S}\frac{dS}{dV}, \qquad (1.)$$

where S is the responsivity of the detector in amps per watt. For small changes in bias, the current flowing in the detector can then be written as

$$I(t) = I_o[1 - aV_{in}(t)], \qquad (2.)$$

where

$$I_o = S_o P + I_{do}. \qquad (3.)$$

S_o and I_{do} represent the responsivity and dark current of the detector under nominal bias conditions and $V_{in}(t)$ is the voltage at the input of the circuit after time t. Analysis of the equivalent circuit shown in figure 1 gives for the output voltage of the circuit at time t after the circuit has been reset,

$$V_{out}(t) = \frac{G}{C} H(t)\, e^{-t/\tau_H}\left[Q_S + \bar{\tau} I_o (1 - e^{-t/\bar{\tau}})\right]. \qquad (4.)$$

Where $H(t)$ is the Heaviside step function, Q_S is the residual charge on the input capacitance of the JF-4 after the circuit has been reset, τ_H is the time constant of the high pass filter and $\overline{\tau}$ is given by

$$\frac{1}{\overline{\tau}} = \frac{1}{\tau} - \frac{1}{\tau_H}. \qquad (5.)$$

Here τ is the effective time constant of the detector and JF-4, given by

$$\tau = \frac{C}{aI_o}. \qquad (6.)$$

Equation 4 can be expanded to second order to give

$$V_{out}(t) = \frac{G}{C}\left[k_0 + k_1 t + k_2 t^2\right], \qquad (7.)$$

where

$$k_0 = Q_s,$$

$$k_1 = I_o\left(1 - a\frac{Q_S}{C}\right) - \frac{Q_S}{\tau_H},$$

$$k_2 = \frac{1}{2}\left[\frac{aI_o^2}{C}\left(1 - a\frac{Q_S}{C}\right) - \frac{Q_S}{\tau_H^2}\right],$$

and initial the current can be estimated from

$$I_o = \frac{k_1 + k_0\frac{1}{\tau_H}}{1 - k_0\frac{a}{C}}. \qquad (8.)$$

A second order fit to the digitised integration ramps should therefore, in principle, be sufficient to derive the initial photocurrent for all illumination levels at which the behaviour of the detector responsivity is accurately represented by equation 1. This photocurrent can then be calibrated as a function of flux by observing a source of known intensity and by measuring the dark current under zero background conditions. In practice, however, deriving the *two* coefficients k_1 and k_2 for nearly linear ramps – that is, those produced under low relatively low levels of illumination with low signal-to-noise – gave rise to excessive noise. To avoid this, the original method of deriving the photocurrent used a linear fit for low fluxes, changing to a second-order fit at a predetermined flux level. However, the consequent swapping of orders introduced an undesirable discontinuity in the calibration that manifested itself either as a step in the final spectrum, or as systematic noise produced when the processing software switched between first and second order from one ramp to the next (*cf.* figure 2). In addition to this problem, the de-biasing factor a also proved difficult to measure and appeared for some detectors to be a function

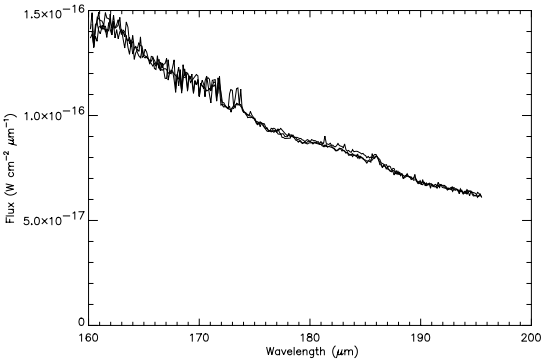

Figure 2: A spectrum where the photocurrent was derived using first and second order fits to the integration ramps. The problem caused by swapping from first to second order can be seen as excess noise in the first portion of the spectrum.

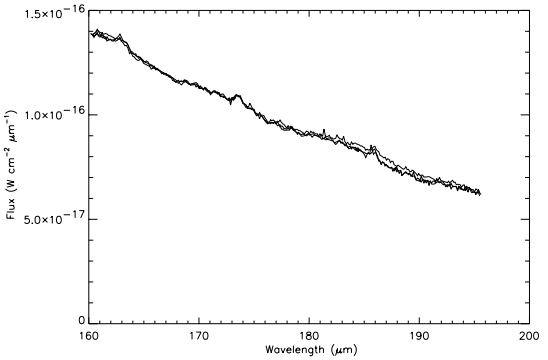

Figure 3: The same spectrum as shown in figure 2, but with the photocurrent derived using the empirical method described in the text. The order swapping problem has now been solved and the spectrum is well calibrated.

of the photocurrent. Finally, the above second-order analysis of the circuit is inadequate at high flux levels.

An empirical method for the derivation of the photocurrent from the voltage ramps has been devised that makes no assumptions about the behaviour of the detectors as they become de-biased and avoids the problems described above. In this method an average effective current is calculated by taking the difference in the charge on the FET gate at two fixed times in the reset period and dividing by the time difference: for a 0.5 second reset these are at 0.055 and 0.49 seconds (sample numbers 6 and 43 out of 44). [In practice, a second-order polynomial was fitted to the charge as a function of time, merely to assist in determining the charge at these two times.] The flux was then derived by reference to the observations of Uranus as described in Swinyard *et al*. (1998). This method makes no *a priori* assumptions about how the detectors respond, but produces well-calibrated spectra with no discontinuities and with lower noise in the reduced spectra (*cf.* figure 3).

2.2 Operating conditions

The nominal operational parameters for the LWS detectors (bias voltage, temperature, reset interval for the JF-4s and number of samples per spectral point) were set during ground testing in the quiescent conditions of the laboratory. The bias voltages for the detectors are given in table 3. We found during ground testing that the value of the NEP itself depended on the length of the reset time; the optimum reset time was found to be greater than two seconds. However, in practice, we thought that it was likely that the impact of ionising radiation would limit the useful reset time to two seconds. All pre-launch performance figures were therefore predicated on the use of two-second reset times. The operating point for each detector bias voltage was set by finding the maximum bias that would not cause the detectors to become unstable (spike

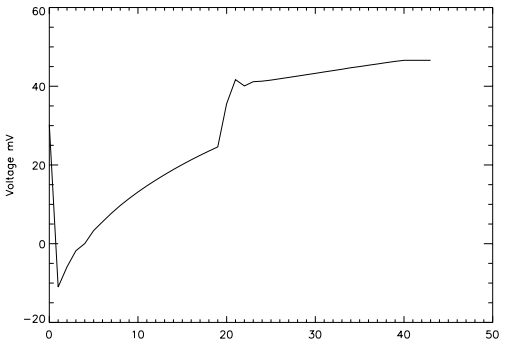

Figure 4: An integration ramp showing the affect on an ionising radiation hit on the detector. A large amount of charge is deposited at the integrating node of the pre-amplifier causing a step in the integration ramp. This step change within an integration ramp can be used to detect and reject bad data.

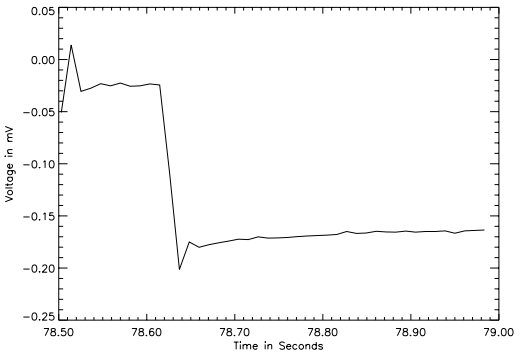

Figure 5: A negative glitch on an integration ramp. These are thought to be caused by an ionising radiation hit on the JF-4 itself.

spontaneously) under the lowest backgrounds achievable in the laboratory. The responsivities determined for these bias settings were then used to derive the instrument performance figures.

When the detectors were operated in orbit, the frequency of ionising radiation hits appeared to be higher than predicted from the pre-launch estimates. On closer inspection, however, we found that the effect of an ionising radiation hit on the detectors was rather different, and more severe, than had been predicted. An ionising particle (either a primary cosmic ray or a secondary generated in the spacecraft structure) could cause the detector to become unstable and spike spontaneously for some seconds following the hit. As the radiation hits, identified from inspection of the integration ramps (see figures 4 and 5) were occurring at intervals of 1 per 8-10 seconds per detector, this meant that the detectors did not recover to a stable operating point between hits. Figure 6 shows an example of the this for the stressed Ge:Ga detector LW2. The result was that, even after the affected integration ramps had been removed from the data stream, the noise was so high that some of the detectors (notably the stressed Ge:Ga types) were practically useless. Experience in the laboratory showed that the spontaneous spiking behaviour in the detectors could be avoided by reducing the detector bias. Figure 7 shows the effect of reducing the bias on the baseline stability of the stressed Ge:Ga detector LW2.

To determine the optimum operating bias for the detectors in orbit, we made a series of measurements on sources of different fluxes with the detectors set at various bias levels. The optimum level was chosen by comparing the average signal-to-noise ratio in the spectrum for each bias level. The bias settings chosen are given in table 2. For all detectors except SW1 and SW2, these are lower than those determined from ground testing. For LW2 the bias was reduced by two command steps, for all others by one command step; one command step corresponding during ground testing to a reduction in responsivity of a factor of two.

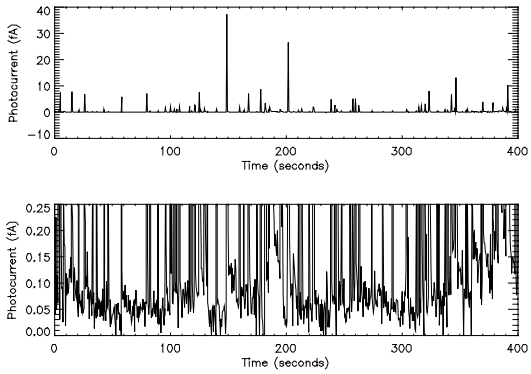

Figure 6: The top panel shows a time series for the stressed Ge:Ga detector LW2 with the bias set to 60 mV under zero illumination conditions. The lower panel shows the same data with the y-scale amplified.

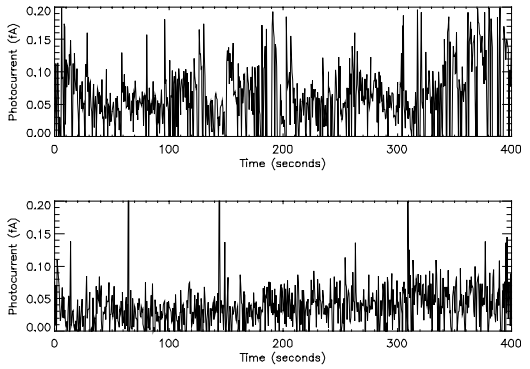

Figure 7: The top panel is the same data as shown in figure 6 with the data points affected by ionising radiation set to 0 (i.e. de-glitched). The lower panel shows a de-glitched time series for the same detector with the bias set at 40 mV – note the better baseline stability.

Even after the bias voltage had been reduced, the detectors were still found to have an increased responsivity for some time following an ionising radiation hit. A study of the decay time following a hit showed that there was no correlation between the size of the measured charge deposit and the length of time required to recover to the nominal responsivity. However, a correlation *was* found between the length of the integration ramp and the number of ramps needed to get back to the nominal responsivity: the shorter the integration ramp, the fewer the number of ramps required for the detector to recover. This led to the use of 0.5 second integration ramps as the nominal with 0.25 second ramps reserved for use with very bright sources where detector saturation was likely.

We investigated whether operating the unstressed Ge:Ga detectors at a higher temperature would improve the recovery time of the detectors after a radiation hit. The detectors were operated at 3.2 K rather than 3 K and the responsivity and dark currents measured. Whilst the responsivity increased by about 20% on average, the dark current increased by a factor of 6 and there was no noticeable improvement in the recovery from ionising radiation hits. Higher temperature operation was not, therefore, implemented.

Extensive tests were carried out on the optimum method of obtaining a spectrum. As stated above, the best method on the ground was to take several integration ramps for each setting of the grating or Fabry-Perot. In this way the time response of the detectors could be properly sampled and corrected for. In orbit this method was found to lead to higher noise in the final spectrum and greater loss of data because the noise in any one spectral sample was now more likely to be correlated as the detector recovered from an ionising radiation hit. We found the optimum method was to take one integration ramp per spectral sample and to build up the total integration time by co-adding repeated scans. In this way the data could be further de-glitched by inter-

comparison of the same spectral sample in all scans. Furthermore, the noise in each spectral sample is nearer to a Poisson distribution.

2.3 Detector Dark Currents

Two long observations of the dark background were taken with the one of the Fabry-Perots in the beam with its etalons set non-parallel. These observations were carried out in revolution 650 on 27 August 1997, at the middle of the revolution and again at the end, some eight hours later. The value and uncertainty of the measured dark currents were determined from a Gaussian fit to the binned data. The values and uncertainties for the 0.5 second reset times are given in Table 1. No significant differences were found between the dark current values derived for 0.25, 0.5 and 1 second resets.

When the LWS was not the prime instrument, useful data from the detectors could still be obtained by using spare portions of the housekeeping telemetry frame to record the output of the detectors at the beginning and end of an amplifier reset period. Much of the time during these "serendipity-mode" operations the LWS was viewing blank portions of the sky and the data could be used to determine the detector dark currents.

Finally, the dark currents could be determined by combining the results of measurements made at the middle of the revolution described in Swinyard *et al.* (1998). There were thus three independent means of measuring the dark currents; they agree with each other to within one or two standard deviations. There appeared to be no significant change in the level of the dark current between the middle and end of a revolution implying that the ionising radiation had no effect on the detector dark currents. This is in disagreement with predictions from tests made during pre-launch calibration (Price *et al.* (1992)).

Detector	Type	Dark current measured in revolution 650 (10^{-16}A)	
		Middle of Revolution	End of revolution
SW1	Ge:Be	4.89±0.42	4.96±0.53
SW2	Ge:Ga(u)	2.15±0.38	2.11±0.40
SW3	Ge:Ga(u)	2.23±0.19	2.31±0.20
SW4	Ge:Ga(u)	1.21±0.30	1.25±0.30
SW5	Ge:Ga(u)	1.63±0.21	1.67±0.22
LW1	Ge:Ga(u)	2.39±0.27	2.63±0.28
LW2	Ge:Ga(s)	0.10±0.22	0.17±0.23
LW3	Ge:Ga(s)	0.49±0.32	0.49±0.34
LW4	Ge:Ga(s)	2.23±0.38	1.94±0.38
LW5	Ge:Ga(s)	1.40±0.22	1.18±0.22

Table 1: Measured values of the detector dark currents. Units are 10^{-16} A in all columns and the uncertainties are quoted as one standard deviation.

2.4 Correction for detector non-linearity.

As described in section 2.1 the flux falling on a detector causes a change in the net bias across the detector. If the flux is high enough that the net bias voltage across it is reduced by a significant fraction (10-20%) of its nominal value, the relationship established between photocurrent and flux using the standard calibration observations becomes invalid and the response of the detector is a strong function of the input flux. An example of this is shown in the upper curve of figure 8. Here, the derived spectrum of a bright source is shown with no correction for non-linear response to high flux levels. Inspection of the complete spectrum showed that the broad absorption features present in the segment of the spectrum measured on this detector are artefacts, as they are not present in portions of the spectrum measured at the same wavelengths on adjacent detectors. The detectors seen to be affected by this non-linear response are the unstressed Ge:Ga detector LW1 and the stressed detectors LW2, LW3 and LW4. The effect begins to be seen at fluxes of around 1000 Janskys at 120 μm.

A model spectrum of Saturn has been calculated by Davis *et al*. (1996) and calibrated against the measured flux in the short wavelength region of the LWS band where the detector response is known to be linear, even at very high flux levels. This spectrum can be multiplied by the instrument response for a single detector to give the *predicted* photocurrent for Saturn over the wavelength region covered by that detector. This model photocurrent is then plotted against the measured current (figure 9), and the degree of non-linearity in the detector response determined.

The fact that the Saturn spectrum is well predicted by modelling, and can be calibrated over some portion of the LWS range, offers a method for the correction of the detector non-linearity for sources with unknown spectra. The dashed line in figure 9 is a quadratic fit to the data. Using the coefficients from this fit, the photocurrent which would have been measured in a completely linear system can be calculated. The calibration is then completed in the same way as with an uncorrected spectrum.

2.5 Detector Performance

The Noise Equivalent Power (NEP) at frequency ν of a photo-conducting detector coupled to an integrating amplifier is given in practical terms by

$$NEP(\nu) = \langle \delta I\,(0.5)^2 \rangle^{1/2} / S(\nu) \quad \mathrm{W\ Hz^{-1/2}}, \qquad (9.)$$

where $\langle \delta I(0.5)^2 \rangle^{1/2}$ is the root-mean squared noise current in amps measured using 0.5 second reset times (equivalent to a 1 Hz bandwidth) and $S(\nu)$ is the detector responsivity in amps per watt. To avoid making assumptions about the transmission of the telescope and instrument the LWS detector responsivity is not measured directly. Instead the instrument response is derived from the measurement of the calibration source (Uranus) and its associated model spectrum; it is given as $S_I(\nu)$ [A cm^2 μm W^{-1}]. We can calculate the Noise Equivalent Spectral Density (NESD) directly from this value:

$$NESD(\nu) = \langle \delta I(0.5)^2 \rangle^{1/2} / S_I(\nu) \quad \mathrm{W\ cm^{-2}\ \mu m^{-1}\ Hz^{-1/2}}. \qquad (10.)$$

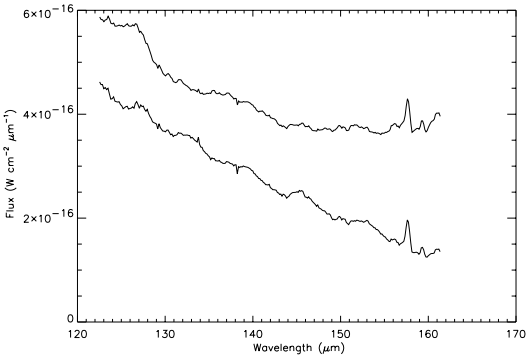

Figure 8: Spectrum affected by detector non-linear response – upper curve. The lower curve shows the same spectrum after correction using the method described in the text.

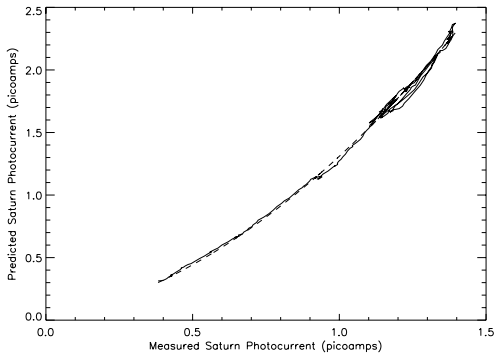

Figure 9: The predicted photocurrent from Saturn model and instrument response plotted against the measured photocurrent. The dashed line is a second order fit used to correct the detector non-linearity.

To convert this to the NEP of the detectors requires knowledge of telescope effective area and the instrument throughput. The instrument throughput was not directly measured on the ground and is complex to calculate. We will, therefore, refer everything to the entrance aperture of the instrument by assuming knowledge of the instrument spectral resolution in grating mode and the effective area of the ISO telescope as a function of wavelength. This effective area has been calculated from an optical model of the ISO telescope and is given for the central wavelengths of each detector in table 2. The spectral resolution of the grating is measured from narrow emission line spectra. The calculated instrument NESD and NEFD (noise-equivalent flux density) figures and the estimated instrument NEP are given in table 2. The in-orbit figures are based on a measurement of the noise under dark conditions taken in revolution 650. To obtain a noise figure 50 minutes of data were taken with the satellite pointing at a dark region of the sky and with a Fabry-Perot in the beam with its etalons set non-parallel. The noise was estimated from the standard deviation of a Gaussian curve fitted to a histogram of the photocurrent values after de-glitching.

A comparison can be made between the instrument NEPs measured during ground testing and those derived in orbit. Inspection of tables 2 and 3 shows that the instrument NEPs have increased by an average of a factor of four in orbit compared to those predicted from ground testing. To understand this increase, it is instructive to estimate the relative contributions from the change in responsivity owing to the reduction in bias and from any increase in the noise. Further inspection of tables 2 and 3 reveals that the average decrease in the responsivity for all detectors is 1.5 and the increase in the noise is 2.8. Some detectors (SW1 and SW2) are operating at the same bias level as on the ground and no change in responsivity is to be expected. The unstressed Ge:Ga (SW3, SW4, SW5 and LW1) are operating 50 mV lower and a factor of two reduction in responsivity is expected; with the exception of LW1, this is approximately what was observed. The stressed Ge:Ga detectors LW3 and LW4 are operating 10mV lower in bias; LW5 20 mV lower and LW2 30 mV. Again, a reduction of a factor of two in responsivity is expected per for LW3, LW4 and LW5 and a factor of four for LW2, based on results from the

ground testing. This has clearly not happened for LW2, LW3 and LW4 and there is a reduction of a factor of three for LW5. Why this should be so is not clear: it is possible that the instrument responsivity was under estimated on the ground or that the presence of ionising radiation causes an increase in the responsivity of these detector types.

The increase in the noise is much more consistent for all detector types. Laboratory tests showed that an increase of a factor of two in NEP is to be expected in going from two-second to the half-second reset times required to minimise the effects of the ionising radiation (Church *et al.* (1993)). In fact the increase in noise is slightly greater than this and the ionising radiation hits are probably contributing excess noise in addition to the read noise of the dark current and the amplifiers.

Detector	Orbit Bias (mV)	Centre λ (μm)	Estimated noise for 0.5 sec resets (10^{-17} A)	NESD (10^{-19} W cm^{-2} um^{-1} Hz$^{-1/2}$)	NEFD (10^{-19} W cm^{-2} Hz$^{-1/2}$)
SW1	600	46.13	4.17	4.43	1.28
SW2	200	56.11	3.83	7.75	2.25
SW3	150	66.03	1.91	3.00	0.871
SW4	150	75.61	2.98	5.40	1.57
SW5	150	84.68	2.13	4.28	1.24
LW1	150	102.25	2.68	0.849	0.509
LW2	40	122.04	2.26	0.231	0.138
LW3	60	141.63	3.19	0.122	0.0734
LW4	60	160.38	3.83	0.202	0.121
LW5	40	177.74	2.21	0.691	0.414

Table 2: Operating parameters and derived performance figures for the LWS detectors in orbit.

Detector	Estimated tel. Effective area (cm^2)	NEP Orbit (10^{-16} W Hz$^{-1/2}$)	Orbit Instrument Resp. (A/W)	Orbit measured $\eta\tau$	Cross over flux (Jy)
SW1	2460	3.16	0.132	0.0046	260
SW2	2431	5.47	0.070	0.0046	1460
SW3	2346	2.04	0.094	0.0095	710
SW4	2262	3.55	0.084	0.0044	1530
SW5	2205	2.74	0.078	0.0044	1330
LW1	1922	0.980	0.274	0.0095	360
LW2	1838	0.254	0.886	0.0095	42
LW3	1838	0.135	2.365	0.0142	28
LW4	1753	0.212	1.803	0.0108	80
LW5	1583	0.656	0.337	0.0033	360

Table 2 (ctd.) : Derived performance figures for the LWS detectors in orbit.

Detector	Ground Bias (mV)	Ground Instrument Resp. (A/W)	Ground noise 2 sec. resets (10^{-17} A)	Dark Current (10^{-16} A)	NEP Ground (10^{-16} W Hz$^{-1/2}$)
SW1	600	0.111	0.77	1.92	0.690
SW2	200	0.081	1.63	0.94	2.02
SW3	200	0.194	1.18	1.77	0.610
SW4	200	0.165	0.90	1.07	0.543
SW5	200	0.139	0.74	1.50	0.531
LW1	200	0.382	1.15	2.77	0.302
LW2	70	0.622	0.80	0.08	0.129
LW3	70	2.352	1.50	0.42	0.0640
LW4	70	1.278	1.54	2.40	0.120
LW5	60	1.061	0.80	3.33	0.0755

Table 3: Ground test performance figures for the LWS detectors.

If the detectors are not photon noise limited then the signal-to-noise ratio is given by

$$\sigma = \frac{P}{NEP}\sqrt{2t}\,, \qquad (11.)$$

where t is the integration time. If the power falling on the detectors is such that the shot noise in the photon stream is the dominant source of noise then the signal-to-noise ratio is given by

$$\sigma = \left(\frac{P}{(4h\nu/\eta\tau)}\right)^{0.5}\sqrt{2t}\,, \qquad (12.)$$

where η is the quantum efficiency of the detector and τ is the throughput of the LWS instrument. The power at which the cross over between read noise and photon noise occurs is given by

$$P_{cross} = \frac{\eta\tau}{4}\left(\frac{NEP^2}{h\nu}\right). \qquad (13.)$$

The signal-to-noise ratio has been calculated for a series of input power levels generated using the internal illuminators in a measurement made on revolution 31 during the ISO in-orbit performance-verification phase. The power from the internal illuminators has been referred to the input aperture of the LWS using the standard calibration tables and the estimated mirror area given in table 2. The data are plotted in figure 10. Also plotted in figure 10 is the predicted behaviour of the signal to noise as a function of input power using the NEP calculated from the noise on the dark current measurement on revolution 650. Where the data deviate from the predicted slope at high input powers, one can assume that the noise has become, or is close to becoming photon dominated. Equation 12 can then be used to estimate the product of the

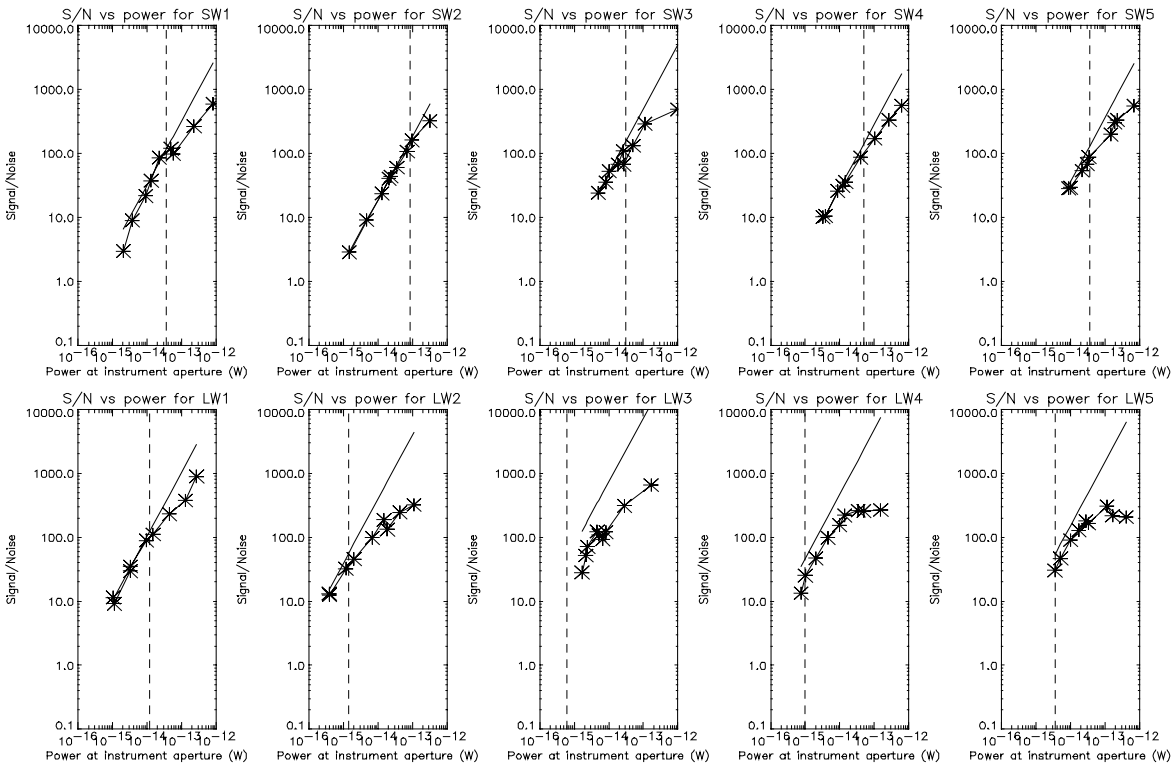

Figure 10: Signal to noise plotted as a function of equivalent power at the entrance aperture of the LWS for each of the LWS detectors. The stars are derived from measurements made using the internal illuminators; the straight solid line is the behaviour predicted from the NEP measured on revolution 650 and the dashed vertical line is the predicted cross over point between read noise and photon noise.

detector quantum efficiency and the instrument throughput, $\eta\tau$. Putting this into equation 13 gives the predicted power at which the noise becomes dominated by the photon shot noise. This cross over power is plotted as a vertical dashed line in figure 10 and is reported in terms of source strength in Janskys in table 2.

In addition to the parameters calculated above, two other factors that determine the detector performance can be estimated from the noise and responsivity measurements: the photoconductive gain, *G*; and excess noise in the dark current. The photoconductive gain can be calculated from

$$G = \frac{Sh\nu}{\eta\tau e}. \qquad (14.)$$

The shot noise in the dark current is given by

Detector	Estimated G	Estimated α	Estimated τ
SW1	0.77	5	0.05
SW2	0.33	15	-
SW3	0.18	8	-
SW4	0.31	4	-
SW5	0.26	1	0.15
LW1	0.35	6	-
LW2	0.94	14	0.05
LW3	1.46	4	-
LW4	1.28	3	-
LW5	0.70	1	0.01

Table 4: Estimated values for the detector photoconductive gain; detector dark current noise term and the instrument throughput

$$<\delta I_D^2> = 4\alpha G I_D e\ , \qquad (15.)$$

where I_D is the dark current and α is an unknown term that represents the extra, unaccountable, contributions to the noise arising from the dark current. The total noise in any measurement is a combination of the shot noise in the dark current and the read noise from the amplifiers themselves, that is,

$$<\delta I_T^2> = <\delta I_D^2> + <\delta I_R^2> \qquad (16.)$$

where $<\delta I_R^2>$ is the noise from the JF-4 amplifiers when there was no bias voltage across the detectors. This was measured in revolution 833. Using the values for the amplifier read noise; the total noise and the detector dark currents, the values of α can be estimated. Table 4 gives the estimated values for G and α. In view of the lack of precision in such measurements, we regard estimated values of up to 4 for α as consistent with unity. On the other hand, the values of α obtained for SW2 and LW2 seem clearly to suggest that we have neglected some source of noise for these detectors and, therefore, possibly for the others whose α exceeds unity. Unfortunately, we do not have a sufficiently homogeneous set of ground-based data to investigate whether this was so before launch.

Church *et al.*(1993) quote estimates of 20% and 40% for the quantum efficiency of the stressed Ge:Ga detectors LW2 and LW5 respectively. They also quote estimates of 9% for a Ge:Be detector and 3% for an unstressed Ge:Ga detector working at 85 μm. Taking these estimates we can calculate an instrument throughput at the central wavelengths of the detectors and these are given in table 4. Whilst the throughput at 85 μm is consistent with expectations, the long wavelength figures are lower and this may indicate that the quantum efficiency of these detectors is rather lower than the estimates given by Church *et al.*(*loc. cit.*).

3 Conclusions

In figure 10 we gave the signal-to-noise ratio for each detector, as a function of input power, predicted using the NEP calculated from a noise measurement made on revolution 650, about two years into the mission. We also plotted the signal-to-noise ratio versus input power as directly measured using the internal calibrators on revolution 31, at the beginning of the mission. The good agreement between the two shows that the performance of the detectors hardly changed during those two years, although there is marginal evidence that the NEPs of the stressed detectors were slightly higher after two years

The comparison of the performance in orbit with that on the ground is more difficult. The presence of ionising radiation certainly increased the responsivity of three of the stressed detectors: at a *reduced* bias the measured responsivity was the *same or greater* than that measured during ground test for LW2, LW3 and LW4. During the mission there were occasions when individual Ge:Ga detectors, both stressed and unstressed, showed an enhanced responsivity for a long period (hours) following a large radiation hit – presumably some form of nuclear interaction – and this may offer some clue as to why the stressed detector responsivity was enhanced. The stressed Ge:Ga detector LW2 also had a permanently lower responsivity after a period when it had been switched off for some weeks – no other detector showed this behaviour. The detector with the highest stress (LW5) appeared to have a much lower responsivity. This may have been a genuine reduction in the performance of the detector, or may reflect the difficulties encountered in the accurate measurement of the responsivity at these long wavelengths during ground test. Even so, inaccuracies in the ground measurement are unlikely to explain the whole of the deficit and we must accept that this detector responded to radiation differently from its peers.

The increased noise of the detectors is largely governed by the need to use shorter integration ramps, so as to ameliorate the effects of the ionising radiation; this increases the NEP by a factor of two. However, as discussed above there appears to be an extra contribution to the noise in-orbit compared with that measured on the ground. This increases the NEP by a further 25% on average for the stressed and unstressed Ge:Ga detectors; for the Ge:Be detector it is nearer a factor of two, probably a consequence of its long recovery time following a radiation hit.

The dark current values quoted for the ground tests should be treated with some caution because it was difficult to measure them in representative conditions. The measurements made with the detectors integrated into the instrument suffered from excess straylight and those made on the individual detectors did not have the same electronics present. Comparisons between the in-orbit values and the ground values are therefore difficult. However, the quoted values for SW1 and SW2 show an increase of a factor of two, and those for the rest of the detectors were about the same. This represents a real increase in the dark current of a factor of two because these detectors are operating at a lower bias and, to first order, the dark current should follow the bias. The dark currents of all the detectors would appear, therefore, to have suffered an initial increase as a result of being exposed to ionising radiation. This increase, and the fact that the dark current did not subsequently change as a function of time like the responsivity, cannot be accounted for by changes in the behaviour of the JF-4s as these only contribute a small fraction of the total dark current.

We conclude that the photoconducting detectors used on the LWS have proved robust and, despite some loss of sensitivity due to the ionising radiation, are well suited to space borne infrared experiments. We would recommend, however, that future missions take into account the following points in the design of their instruments

1. The volume of the detectors should be minimised to reduce the radiation cross section even at the cost of some loss of dynamic range – this can be recovered by, for instance, the use of filters.

2. The speed of recovery of the detectors from an ionising radiation hit should be as fast as possible, even at the sacrifice of responsivity or instantaneous NEP.

3. Ionising radiation in space *will* increase the NEPs of photoconducting detectors compared to measurements made in ground testing. In the case of the LWS the increase was about 25% for most detectors when all known factors were taken into account. In other cases the amount of the increase will depend on the particular design of the detectors and read out electronics.

4. Although the use of integrating amplifiers leads to de-biasing of the detectors, this can be calibrated out. The short integration ramps can be used to reduce the recovery time of the detectors following a radiation hit and have been essential in the removal of bad data in the final LWS spectra.

4 Acknowledgements

ISO is an ESA project with instruments funded by ESA Member States (especially the PI countries: France, Germany, the Netherlands and the United Kingdom) and with the participation of ISAS and NASA. S.J. Leeks acknowledges the receipt of a U.K. Particle Physics and Astronomy Research Council award.

References

Church, S.E., Griffin, M.J., Ade, P.A.R., Price, M.C., Emery, R.J., Swinyard, B.M. (1993), "Calibration and Performance of Doped-Ge Photoconductors for the ISO Long Wavelength Spectrometer", Infrared Phys. **34**, pp389-406

Clegg P., *et al.* (1996), "The ISO Long-Wavelength Spectrometer", A&A **315**, pp L38-42

Davis, G.R., *et al.* (1996), "ISO LWS measurement of the far-infrared spectrum of Saturn", A&A **315**, ppL393-396

Lim T., *et al.* (1998), "Long term performance of doped Ge:Ga photoconductors in the space environment", in *Infrared Astronomical Instrumentation,* SPIE **3354**, in press.

Price M.C., Griffin, M.J., Church, S.E., Murray, A., Ade, P.A.R. (1992), "Ionising Radiation-Induced Effects in Doped Germanium FIR Photoconductors", *Proc. of ESA Symposium on Photon Detectors for Space Instrumentation,* ESA SP-356, pp309-312

Swinyard, B.M., *et al.* (1996), "Calibration and performance of the ISO Long-Wavelength Spectrometer", A&A **315**, pp L43-48

Swinyard, B.M., *et al.* (1998), "In-orbit performance of the ISO Long Wavelength Spectrometer", in *Infrared Astronomical Instrumentation,* SPIE **3354**, in press. 1998